Available online at www.sciencedirect.com
ScienceDirect
Remote Sensing of Environment 107 (2007) 223–231
Remote Sensing of Environment
www.elsevier.com/locate/rse

Near-surface wind speed retrieval from space-based, multi-angle imaging of ocean sun glint patterns

David Fox [a,1], Enrique Gonzalez [a,2], Ralph Kahn [b,*], John Martonchik [b]

[a] Glendale College, Glendale, CA, United States
[b] Jet Propulsion Laboratory, California Institute of Technology, 4800 Oak Grove Drive, Pasadena CA 91109, United States

Received 15 August 2006; received in revised form 3 October 2006; accepted 21 October 2006

Abstract

The relationship between the MISR multi-angle observations of sun glint pattern width over ocean and the near-surface wind speed is explored. With this relationship, we develop an algorithm that can constrain the standard, wind-driven glint/white cap model that defines the ocean–surface boundary condition in MISR aerosol retrievals. The key geometric factor determining wind retrieval quality is the angular distance between the reflection vector and the closest MISR multi-angle observation — the minimum Sun Glint Angle (SGA).

MISR-retrieved winds are within 2.4 m/s of buoy-measured values for minimum SGA below about 15° for the 38 cases studied, and usually better than 1.1 m/s, except one for which the wind speed was extremely low. For minimum SGA above about 15°, MISR angular glint pattern reflectance sampling is not adequate to perform wind retrievals. An ambiguity in the retrieval that can occur for minimum SGA greater than 6° or 7° is resolved by the minimum observed absolute reflectance. We also confirm the high accuracy of the Cox–Munk ocean surface reflectance model, used to analyze the glint pattern dependence on wind speed. The wind-retrieval method could be used in an operational multi-angle aerosol retrieval algorithm to dynamically constrain the ocean surface boundary condition when glint pattern angular sampling is adequate.

Keywords: Sun glint; Ocean wind speed; Multi-angle remote sensing; MISR; Aerosol retrieval

1. Introduction

The Multi-angle Imaging SpectroRadiometer (MISR) flies aboard the NASA Earth Observing System's Terra spacecraft, in Sun-synchronous orbit, at an altitude of about 704 km. Retrieving atmospheric aerosol amount and type, by means of their light-scattering properties, are among the principal contributions of this instrument. Complicating this analysis is the reflection from Earth's surface.

Over the ocean, surface reflectance is significantly affected by the extent of whitecaps, which is driven primarily by the surface wind speed. Specifically, as wind speed increases, the fraction of ocean surface covered by whitecaps increases (Koepke, 1984). This increases the reflectance by about the same amount for all visible spectral bands, and produces an increase of smaller magnitude in the near-infrared bands (Frouin et al., 1996; Moore et al., 2000). Also with increased wind speed, the impact of view angle on surface reflectance usually decreases — the angular reflectance curve becomes flatter, and any specular reflection peaks (glint features) broaden, since the increasingly multifaceted surface tends toward a lambertian reflector.

Most often, reflectance values at the top of the atmosphere (TOA) are highest for the most oblique viewing angles, due to the large atmospheric scattering contributions for these high air mass factors, and decrease toward the nadir; any sun glint peak is superposed on this pattern, and usually affects the near-nadir-viewing MISR cameras.

If MISR observations can be used to evaluate the ocean surface wind speed, even crudely, they can help constrain ocean surface reflectance, thereby improving MISR aerosol retrievals. Fortunately, the angular distribution of radiance from sun glint off the water's surface also depends on the wind speed. We explore in this paper the relationship between the angular radiance signature of glint patterns over ocean, as resolved by MISR's nine cameras, and the near-surface wind speed. Breon

* Corresponding author.
E-mail address: Ralph.Kahn@jpl.nasa.gov (R. Kahn).
[1] Now at U.C. Berkeley, Berkeley, CA.
[2] Now at CalPoly Pomona.

0034-4257/$ - see front matter © 2007 Elsevier Inc. All rights reserved.
doi:10.1016/j.rse.2006.10.021

and Henriot (2006) pursue a similar idea for POLDER (POLarization and Directionality of the Earth's Reflectances) satellite observations. POLDER uses a fisheye lens to collect data at many more angles than MISR, providing better glint pattern angular resolution, and allowing both wind speed and wind direction retrievals.

We develop empirical relationships by associating observed MISR radiance patterns with coincident, direct measurements of surface wind speed from deep-ocean buoys. We also compare the MISR TOA radiance patterns with those simulated using a standard Cox–Munk model that takes account of sun geometry, viewing geometry, and wind speed (Cox & Munk, 1954; Kahn et al., 2001; Martonchik et al., 1998). We find that the minimum observed sun glint angle is usually the limiting factor in determining the wind speed over the ocean surface from MISR data. The wind speeds derived for cases under 15° minimum Sun Glint Angle (SGA) are accurate to within 2.4 m/s, and usually better than 1.1 m/s, of the wind speed measured by moored buoys, except for wind speeds below about 1 m/s. (SGA is the angle between the solar beam specular reflection vector, referenced to a flat ocean surface, and a vector pointing to the camera; the minimum SGA is the SGA for the camera viewing closest to the specular reflection vector.) This study also provides evidence that the Cox–Munk model is an accurate indicator of reflectance when compared to MISR observations, similar to the POLDER analysis results (Breon & Henriot, 2006). We propose an operational algorithm that could provide wind speed constraints for a glint and white cap model like the one used in the MISR algorithm, and assess its capabilities and limitations.

2. Data description

MISR has nine cameras, pointing at multiple angles, oriented roughly along the spacecraft line-of-flight. This enables MISR to image, within about seven minutes, a 400-km-wide swath of Earth's surface at nine different view angles, ranging from about

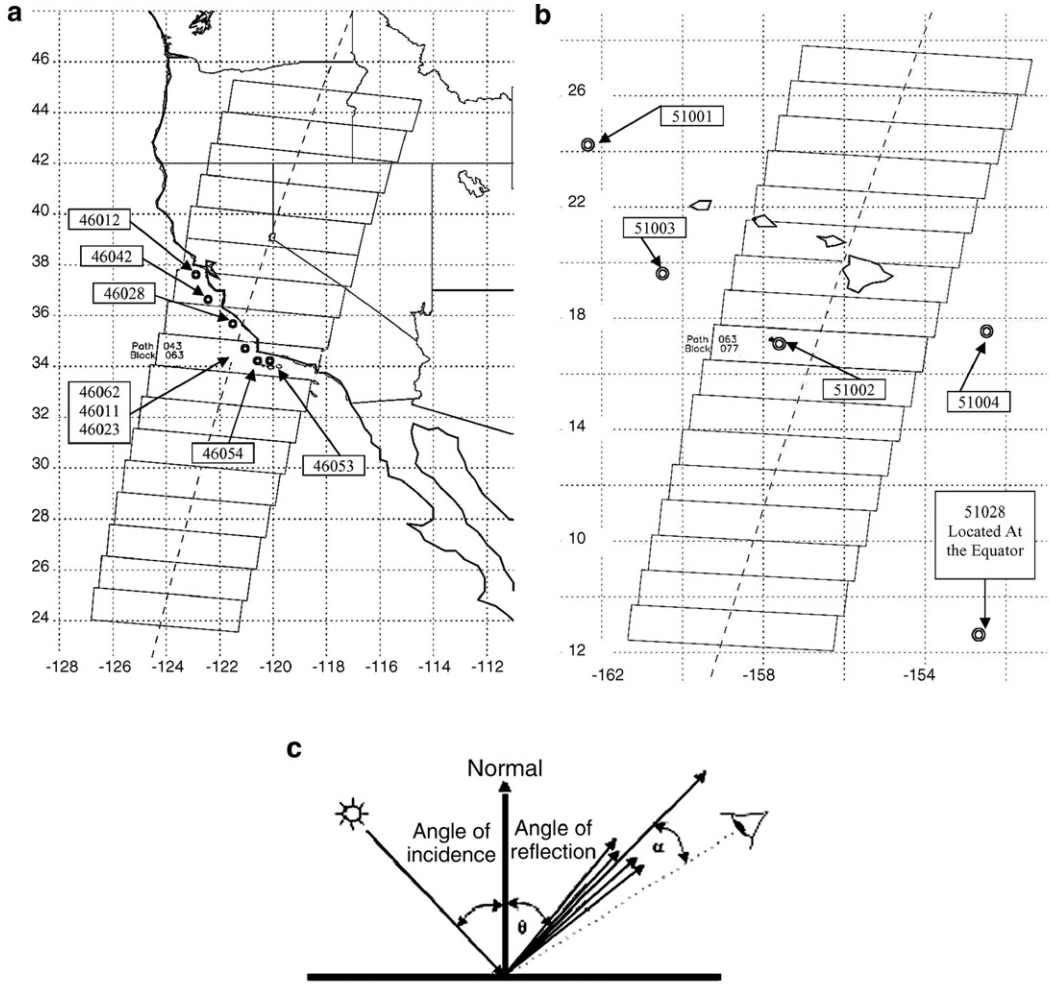

Fig. 1. Buoy locations and Sun Glint Geometry. (a) Approximate locations of NOAA buoys (open circles) along the California coast used for this study, superposed on a map of state boundaries and a sample MISR swath coverage (Orbit 1475, Path 043, 18:56 UTC on September 26, 2002). MISR image blocks are shown as rectangles, and the sub-spacecraft track is marked with a dashed line. Table 2 lists the buoy latitudes and longitudes. (b) Same as (a), but for the group of buoys near Hawaii used in our investigation. MISR coverage for Orbit 2221, Path 064, 21:24 UTC on May 18 2000 is also shown in this illustration. Note that Buoy 51028 is actually located at the equator, but is plotted here for comparison. (c) The angles of solar incidence and reflection are given as (θ), and the Sun Glint angle (α) lies between the specular reflection vector and the MISR camera viewing direction.

70° forward, through nadir, to 70° aft, as the spacecraft passes overhead (Diner et al., 1998). MISR reports top-of-atmosphere radiance in four spectral bands, including three visible and one near-infrared wavelength of 446, 558, 672, and 867 nm, respectively.

The National Oceanographic and Atmospheric Administration (NOAA) National Data Buoy Center (NDBC) provides historical reports of wind speed measured at moored ocean buoys. We chose eight buoys along the California coast near San Francisco (Fig. 1a); there were many buoys in that area, and it is possible to compare similarities among nearby ones. Five additional buoys near Hawaii were selected to provide data for deep ocean cases (Fig. 1b). For eleven of the buoys, wind speed is measured at 5 m above sea level, and for the other two buoys (46023 and 46054), the measurement is at 10 m above sea level (see Table 2).

MISR radiance data (Level 1B2 MISR Standard Products, distributed by the NASA Langley Atmospheric Sciences Data Center http://eosweb.larc.nasa.gov) were collected for cloud-free, 3 × 3 1.1-km-pixel patches, centered on the location of each buoy to within half a pixel. The MISR near-infrared (NIR) data is used in this paper, because of its greater sensitivity to surface reflection in the presence of atmosphere than the shorter wavelength bands. Coincident wind vectors were collected for the buoy locations through the Historical Wind Speed Measurements provided by the NDBC website (http://www.ndbc.noaa.gov). The wind speed was averaged over ±2 h of MISR overpass time, during which it typically varied by about one meter per second. The data sets cover observations from April 2000 to November 2002, and they include reported four-hour average wind speeds well distributed between 0.5 and 11.3 m/s (Table 1).

Table 1
MISR-buoy coincident events, listed in increasing minimum SGA order, along with the sequence of model reflectance curve peaks

Minimum SGA	Observed wind (m/s)	Date	Time (UTC)	NOAA buoy #	Terra orbit	MISR V#†	Wind speeds ordered by model reflectance peak, from highest to lowest§															Reflectance order notes
6.4528	6.2	5/31/00	20:58:18	51028	2410	0020	**0**	1	2	**3**	4	5	6	7	8	9	10	11	12	13	14	15	
7.8236	5.0	9/02/00	21:05:18	51004	3779	0020	**1**	0	2	**3**	4	5	6	7	8	9	10	11	12	13	14	15	
8.3628	6.2	5/15/00	20:58:02	51028	2177	0020	**1**	2	3	**0**	4	5	6	7	8	9	10	11	12	13	14	15	
8.367	4.5	7/18/00	20:57:55	51028	3109	0020	**1**	2	3	**0**	4	5	6	7	8	9	10	11	12	13	14	15	
8.8379	9.4	8/17/00	19:20:51	46042	3545	0020	**1**	2	3	4	**0**	5	6	7	8	9	10	11	12	13	14	15	
9.2631	5.7	4/28/00	21:48:09	51001	1930	0020	**1**	2	3	**0**	4	5	6	7	8	9	10	11	12	13	14	15	
9.4638	10.3	9/17/02	19:01:45	46062	14627	0017	**1**	2	3	4	5	**0**	6	7	8	9	10	11	12	13	14	15	
9.4938	3.6	9/10/02	18:55:48	46053	14525	0020	**1**	2	3	4	5	6	7	**0**	8	9	10	11	12	13	14	15	
11.073	0.5	5/18/00	21:24:06	51002	2221	0020	**1**	0	2	**3**	4	5	6	7	8	9	10	11	12	13	14	15	
11.489	8.4	7/07/02	21:33:36	51001	13580	0017	**1**	2	3	4	5	6	7	8	9	10	11	12	13	14	15	**0**	0 m/s lowest
12.06	4.7	5/04/02	21:33:19	51001	12648	0017	**2**	1	3	4	5	6	7	8	9	10	11	12	13	14	15	**0**	
12.064	9.0	7/23/02	21:33:36	51001	13813	0017	**2**	1	3	4	5	6	7	8	9	10	11	12	13	14	15	**0**	
12.101	7.5	8/18/00	21:46:46	51001	3561	0020	**2**	1	3	4	5	6	7	8	9	10	11	12	13	14	15	**0**	
12.233	2.1	11/18/01	21:31:03	51003	10216	0018	**2**	1	3	4	5	6	7	8	9	10	11	12	13	14	15	**0**	
12.59	9.4	7/21/00	21:24:00	51002	3153	0020	**2**	3	1	4	5	6	7	8	9	10	11	12	13	14	15	**0**	
13.052	6.6	8/17/00	19:20:43	46012	3545	0020	**3**	2	4	5	6	7	**1**	8	9	10	11	12	13	14	15	**0**	
13.476	8.7	8/19/00	20:57:40	51028	3575	0020	**3**	2	4	5	6	7	**1**	8	9	10	11	12	13	14	15	**0**	
13.773	9.0	8/08/02	21:33:21	51001	14046	0017	**2**	3	4	5	**1**	6	7	8	9	10	11	12	13	14	15	**0**	
13.942	6.6	3/10/00	21:05:06	51004	1216	0019	**3**	2	4	5	6	**1**	7	8	9	10	11	12	13	14	15	**0**	
14.116	3.0	9/10/02	18:55:50	46054	14525	0022	**3**	4	**2**	5	6	7	8	9	10	11	**1**	12	13	14	15	**0**	
16.302	5.9	4/13/00	20:58:15	51028	1711	0020	4	5	**3**	6	7	8	**2**	9	10	11	12	13	14	15	**1**	0	1 m/s next lowest
19.274	7.5	11/07/00	20:56:10	51028	4740	0020	5	6	7	4	8	9	**3**	10	11	12	13	14	15	**2**	1	0	
19.336	3.1	9/10/02	18:55:45	46023	14525	0022	6	7	8	5	9	10	11	12	4	13	14	15	**3**	2	1	0	
19.514	1.9	9/10/02	18:55:42	46011	14525	0022	6	7	8	5	9	10	11	12	13	4	14	15	**3**	2	1	0	
20.46	2.7	10/03/02	19:01:18	46028	14860	0017	9	10	8	11	15	12	14	13	7	6	5	4	**3**	2	1	0	
21.265	2.9	9/10/02	18:55:39	46062	14525	0017	8	9	10	7	11	15	12	14	13	6	5	4	**3**	**2**	**1**	0	
25.823	8.1	7/30/01	20:44:40	51028	8599	0018	15	14	13	12	11	10	9	8	7	6	5	4	**3**	**2**	**1**	**0**	Order completely
27.627	5.9	9/14/01	20:50:22	51004	9269	0018	15	14	13	12	11	10	9	8	7	6	5	4	**3**	**2**	**1**	**0**	reversed
29.371	4.9	11/17/01	20:48:21	51004	10201	0018	15	14	13	12	11	10	9	8	7	6	5	4	**3**	**2**	**1**	**0**	
29.627	5.3	9/10/02	18:55:33	46028	14525	0017	15	14	13	12	11	10	9	8	7	6	5	4	**3**	**2**	**1**	**0**	
29.722	6.8	10/15/00	20:50:37	51028	4405	0020	15	14	13	12	11	10	9	8	7	6	5	4	**3**	**2**	**1**	**0**	
30.675	11.3	3/19/00	20:59:21	51004	1347	0019	15	14	13	12	11	10	9	8	7	6	5	4	**3**	**2**	**1**	**0**	
30.719	2.3	11/05/02	21:26:53	51001	15342	0017	15	14	13	12	11	10	9	8	7	6	5	4	**3**	**2**	**1**	**0**	
31.226	7.7	4/26/01	21:24:41	51003	7216	0018	15	14	13	12	11	10	9	8	7	6	5	4	**3**	**2**	**1**	**0**	
32.621	6.9	10/31/00	20:50:00	51028	4638	0020	15	14	13	12	11	10	9	8	7	6	5	4	**3**	**2**	**1**	**0**	
34.05	8.7	3/24/00	21:18:19	51002	1420	0020	15	14	13	12	11	10	9	8	7	6	5	4	**3**	**2**	**1**	**0**	
34.209	7.7	10/19/01	21:20:10	51003	9779	0018	15	14	13	12	11	10	9	8	7	6	5	4	**3**	**2**	**1**	**0**	
35.855	1.7	3/30/02	21:04:21	51002	12138	0016	15	14	13	12	11	10	9	8	7	6	5	4	**3**	**2**	**1**	**0**	

†MISR Level 1B2 Radiance Product Version Number.
§These columns list the wind speeds associated with the model reflectance curves, in order of decreasing reflectance peak height, starting with the one having highest peak for the geometry of that observation.
Numbers in bold highlight significant changes in the ordering.

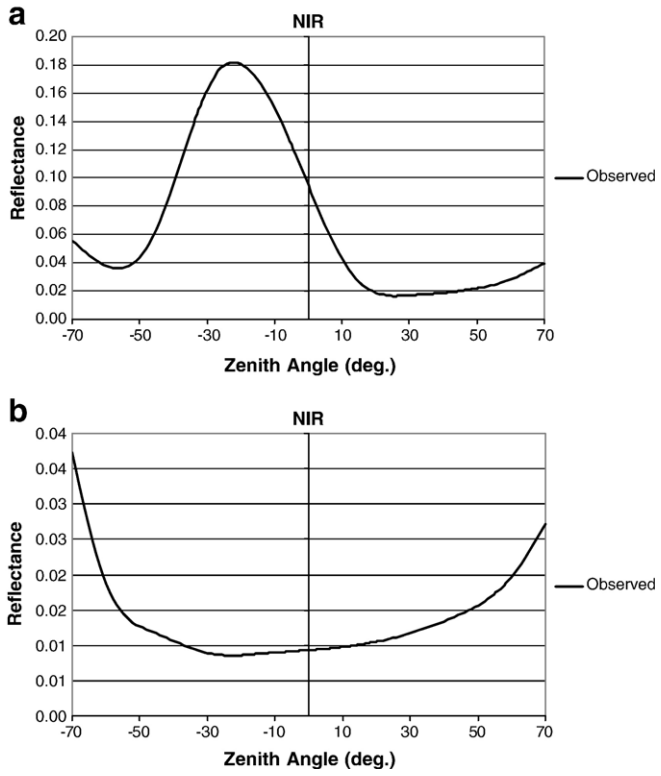

Fig. 2. Examples of MISR near-infrared band reflectance vs. view zenith angle curves, interpolated to a 1° grid over the view zenith range −70° to +70°. (a) Observed reflectance curve for a case having a minimum SGA of 9.5° and a well-defined sun glint peak. (b) Observed reflectance curve for a case where no camera is near the Sun's specular reflection (minimum SGA=38.9°), so virtually no sun glint peak is observed.

Geometry and radiometry data were extracted from MISR Level 1B2 Data files, following Kahn et al. (2001). The geometry data include view zenith and azimuth angles of each camera and of the Sun's specular reflection vector, as well as calculated SGA and spectral reflectance values for each camera. The geometry is illustrated in Fig. 1c.

3. Wind retrieval analysis

To explore the correlation between the MISR-observed and model reflectance curves, the behavior of the Cox–Munk modeled reflectances are first studied alone. Once the pattern of modeled cases is characterized and explained, the MISR-observed reflectances are compared.

3.1. Behavior of model peak reflectances

For each MISR observation, the nine camera NIR (867 nm) reflectances were interpolated with respect to view zenith angle using a cubic spline, to generate reflectance values for every 1° of view zenith. The result is a Reflectance vs. View Zenith Angle curve to compare with model simulations. For clarity, we assign negative zenith angle values to the MISR forward-viewing cameras, positive values to the aft-viewing cameras, and for the nadir camera, whichever sign puts it closer to the center of the plot. Examples, sampled at 1° intervals, are shown in Fig. 2a, which has a well-defined glint peak due to the low minimum SGA of 9.5°, and Fig. 2b, where the minimum SGA is 38.9° and the sun glint peak is not captured in this geometry.

Simulations were made of top-of-atmosphere (TOA) radiance (Martonchik et al., 1998) for the nine cameras, using the same view and sun geometry as the MISR observations at the buoy sites. A version of the Cox–Munk model (Cox & Munk, 1954) was used for water surface reflectance in which the reflectance is not dependent on wind direction. The atmosphere was modeled assuming Rayleigh scattering defined by surface pressure for a standard atmosphere and aerosol scattering in the lower atmosphere using a mixture of 0.12 and 2.8 μm effective radius spherical, non-absorbing particles with a mid-visible column optical depth of 0.1 (with the smaller particles contributing ~90% of the aerosol optical depth). The simulations were performed for 16 ocean near-surface wind speeds, ranging from 0 to 15 m/s, in 1 m/s increments. The simulated TOA radiance values were then converted to equivalent reflectance values and interpolated to 1° view zenith resolution. The result is a set of simulated Reflectance vs. View Zenith curves, for each MISR observation, at the 16 designated surface wind speeds.

Fig. 3 illustrates typical model behavior when the minimum SGA is less than about 7°. For low wind speeds, the curves have pronounced peaks with high maximum reflectance, whereas for high wind speed cases, they have broadened peaks with low maximum reflectance. The reflectance of the low wind speed curves is seen to drop below zero on either side of the glint peak, due to the cubic spline fit to the simulations overshooting between the calculated points. This feature of the curves was accounted for in the analysis described later.

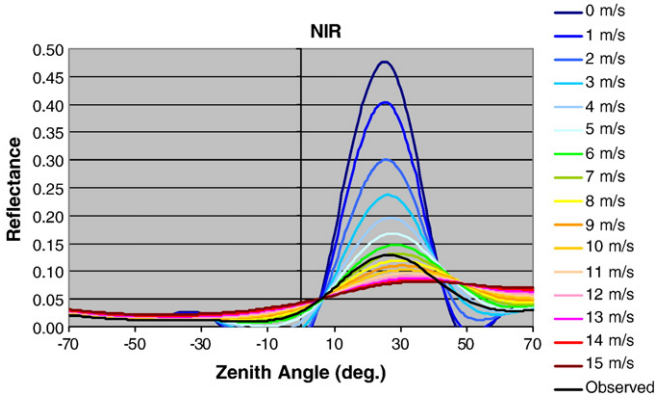

Fig. 3. Simulated Cox–Munk model curves, and the related MISR observations curve, for small minimum SGA, illustrated by a 6.2 m/s MISR event geometry, having minimum SGA=6.45°. The lowest modeled wind speeds have the tallest and sharpest peaks, whereas the highest wind speed cases have the lowest and broadest peaks. Note also how the MISR observations peak just below the 7 m/s model curve. The right column displays the colors corresponding to the model wind speeds. MISR observations are shown in black, and "NIR" refers to the MISR near-infrared channel used in this and other figures. [The plotted reflectance curves near the minima go negative as a consequence of numerical overshoot in the cubic spline fitting; the model itself does not produce negative values.]

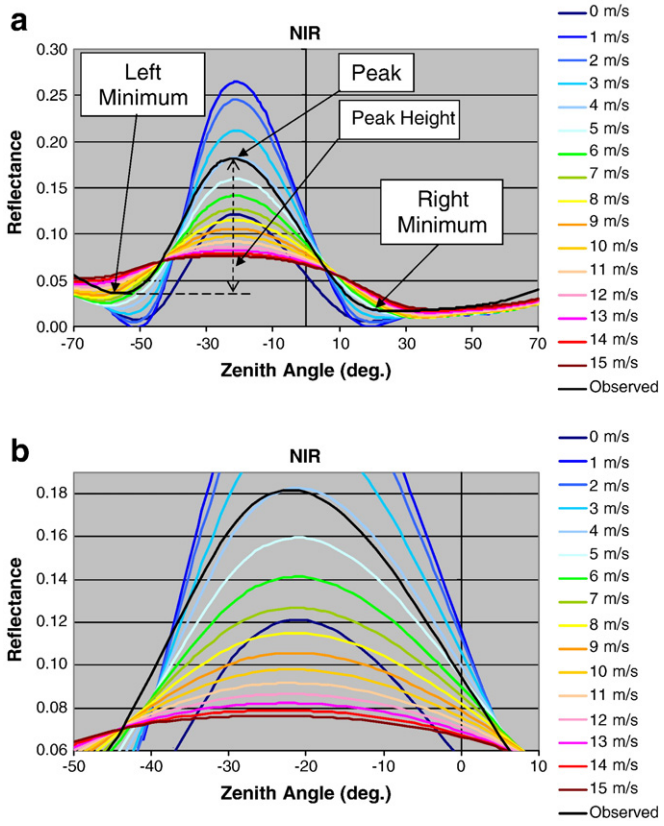

Fig. 4. (a) Simulated Cox–Munk model curves, and the related MISR observations curve, for moderate minimum SGA, illustrated by the 3.6 m/s MISR event geometry, having minimum SGA=9.49°. For the MISR curve, the local maximum and minima, used for measuring the radiance curve widths, are labeled, and the Peak Height is shown as being the difference in reflectance between the maximum and, in this case, the left minimum, since it is the brighter of the two. (b) Close-up view of part (a), showing how the model 0 m/s wind speed falls between model 7 m/s, and 8 m/s wind speeds. Note also how the MISR observations peak just below the 4 m/s modeled curve. The right column displays the colors corresponding to the model wind speeds. MISR observations are shown in black.

As the minimum SGA increases, the pattern of model wind speed reflectance curves changes as a consequence of the altered geometry. Glint peaks still become progressively shorter and broader as wind speed increases, but the curve representing the lowest wind speed is not the top-most peak (Fig. 4). The lowest modeled wind speed (0 m/s) now falls lower among the modeled set of curves, between the 7 m/s and 8 m/s plots (Fig. 4b). This 0 m/s model curve transition begins when the minimum SGA is about 6.5°. The 1 m/s model curve begins its transition toward lower reflectance peaks at a minimum SGA of approximately 12°. This occurs because, as the minimum SGA increases, the MISR cameras now sample the sides and base of the glint pattern, and not as close to the peak. Since glint patterns for lower wind speeds are taller, narrower, and steeper than those for larger wind speeds, there is a view angle threshold beyond which the higher wind speed's glint pattern has values larger than those for the lower wind speed's pattern. The glint patterns in Fig. 4 demonstrate this threshold crossover.

More generally, Table 1, showing all 38 MISR-Buoy coincident cases, is organized by minimum SGA to highlight the pattern of model curve transitions as the minimum SGA increases. Every modeled case is run for the minimum SGA and other geometry of the corresponding MISR observation. The numbers 0 through 15 are the modeled wind speeds, arranged from left to right in order of decreasing peak reflectance for that case. The key element illustrated by this table is the effect that the minimum SGA has on reflectance curve appearance and information content.

At intermediate minimum SGA, ranging from about 7° to 21°, the model curves for higher wind speeds retain their original ordering, whereas those for lower wind speeds appear between the higher model wind speed curves; with increasing minimum SGA, each modeled low wind speed curve moves progressively toward lower reflectances, becoming shorter and broader.

For minimum SGA larger than between 20° and 25°, the wind speed curve order reverses completely, and low wind speed model curves may have no measurable peaks at all. In this situation, there is no camera near enough to the specular reflection vector to produce a strong specular signal, even when the water is calm. Instead, higher peaks result from more dispersion of sunlight toward the camera's direction by ocean surface facets, an effect enhanced by higher wind speed conditions.

Note also that the 0.5 m/s case is the only one that does not follow this trend. We have not specifically identified the cause of this anomaly, but for extremely low wind speeds, especially in the glint region, small deformations of the nearly flat ocean surface can produce large optical effects. In particular, perturbations by a wind gust or other effect are not included in the Cox–Munk model, but they are more likely to significantly alter the surface-scattered-light pattern of an unusually smooth ocean surface than similar perturbations of the generally rougher ocean surface.

The apparent transition of the lower model wind speeds, toward lower peak reflectance levels as the minimum SGA increases, considerably complicates the wind retrieval process.

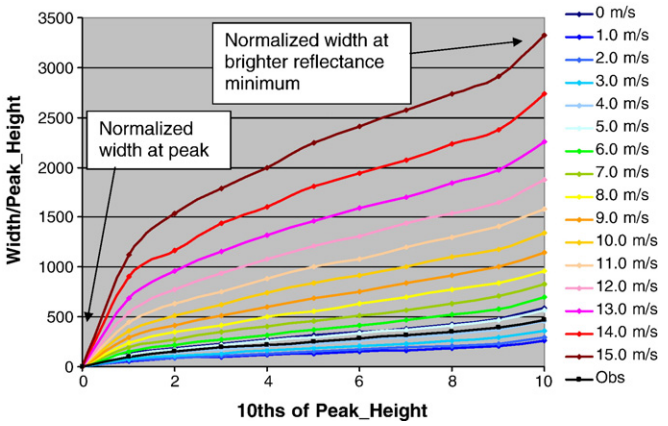

Fig. 5. Measured width/(peak height) ratio, reported in units of degrees/[reflectance fraction] at intervals of tenths of the peak height, for the 3.6 m/s MISR event geometry (minimum SGA=9.49°). Each reflectance curve was measured individually.

3.2. Behavior of model reflectance width/height ratio

Atmospheric and water conditions can also affect both the baseline reflectance and peak reflectance of the observations. However, the width of the glint pattern, rather than the height, was found to be a more robust indication of wind speed, when the model curves were tested against the observations.

Each observation and the corresponding set of model reflectances were analyzed numerically to find the sun glint peak view zenith angle and maximum reflectance, and to determine the view zenith angle locations and reflectances of the two local minima defining the boundaries of that peak (e.g., Fig. 4a). This was done using custom functions programmed in Excel: starting at the zenith angle of the most near-specular viewing camera, zenith-angle-adjacent reflectance values were compared to identify the direction of increase. This direction was then searched, by comparing adjacent reflectance values, to determine the inflection point, which was designated the peak maximum. Starting at *this* point, both sides of the curve were then searched away from the maximum to determine the inflection points defining the minima. For model curves where a distinct maximum and minima could not be determined by this method, that curve was designated "not measurable" and was excluded from subsequent consideration (see Fig. 6); in cases where the MISR observation curve was not measurable, no wind speed retrieval was attempted. Figs. 2a, 3, and 4 are examples of radiance curves with well-defined sun glint peaks, for which wind retrievals can be performed, whereas Fig. 2b shows a case having no measurable sun glint peak.

To compare the observed and modeled reflectance curves, we divided each glint feature into tenths along the reflectance axis, from the top of the peak (0/10ths) to the brighter of the two surrounding local minima (10/10ths), and measured the glint feature angular width at each tenth. We then normalized the widths by the peak "height," defined as the reflectance difference between the peak and the brighter of the two surrounding local minima (plotted in Fig. 5 for the 3.6 m/s MISR event). Finally, we linearly regressed the normalized

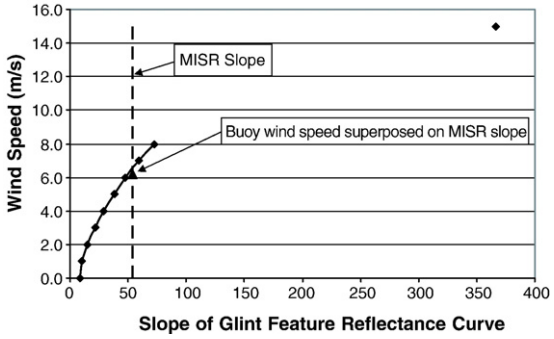

Fig. 6. Unambiguous case. Slope of each model wind speed width/(peak height) curve for the 6.2 m/s MISR event geometry with a minimum SGA of 6.45°. In this case, no transition takes place, and the curve is monotonic in wind speed. Model slopes for wind speeds of 9–14 m/s are absent; in this case, curves could not be measured as described in Section 3.2 and illustrated in Fig. 3, because the right-side minimum could not be determined (see text). The MISR observation slope is represented as a dashed vertical line, with a triangle indicating the buoy-measured measured wind speed.

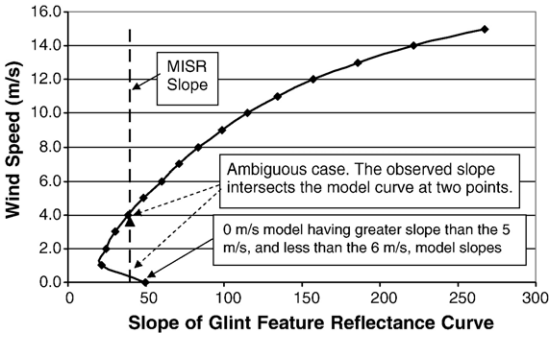

Fig. 7. Ambiguous case. The 3.6 m/s MISR event, having minimum SGA of 9.49°.

widths against their locations (defined as the number of tenths, of the peak height) for each event, and reported the slopes (e.g., Figs. 6, 7, and 8, discussed in the next section). Such a linear regression slope was determined for each hypothetical wind speed, Cox–Munk model, as well as for the observation.

It must be emphasized that these slopes, and all references to the word "slope" hereafter in this paper, pertain to such plots of normalized width measurements, versus their locations (as illustrated in Fig. 5); they do *not* describe the slope of the reflectance curve itself. Thus, large slopes correspond to rapidly widening Sun-Glint features, whereas small slopes correspond to sharper peaks, inasmuch as there is a smaller rate-of-change, in width measurements, for this kind of Sun-Glint feature.

3.3. Comparisons between models and data

Retrieved wind speeds are principally determined by identifying the simulated wind speed model whose slope is most similar to that of the MISR observation. Fig. 6 presents an example of a low minimum SGA case, 6.45° (reflectance curves for this case are illustrated in Fig. 3). The slopes of all the models are in sequence, and there is only one branch to the curve representing the plotted slopes vs. associated wind speeds of the models. The vertical line in this graph is the constraint provided by the slope calculated from the MISR observations. The triangle, which we placed on the vertical line, shows the four-hour average wind speed actually measured by the moored buoy at the time of the MISR flyover.

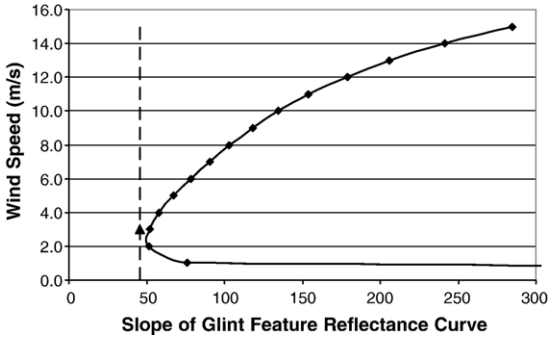

Fig. 8. Case where the MISR-observed slope is smaller than all model slopes. The minimum SGA is 14.1°.

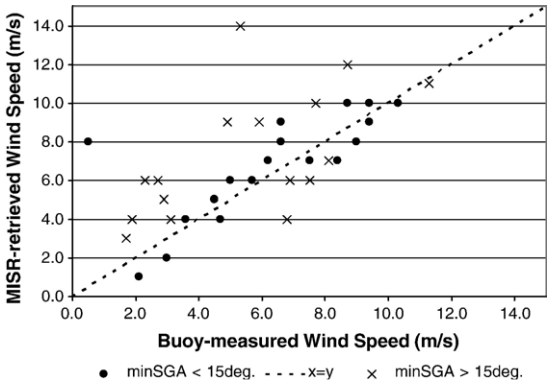

Fig. 9. MISR Ocean Surface Wind Retrieval Result Summary. Cases having minimum SGA below 15° are displayed as filled circles, and those having larger minimum SGA are displayed as X's. Only 34 cases are visible because the results for four pairs of cases (at 5.9, 6.2, 7.7, and 9.0 m/s) are superposed. Table 2 gives a numerical summary of all cases.

The wind speed is determined unambiguously as about 7 m/s for this event. Such a straightforward determination tends to occur for minimum SGA below about 7°. The wind speed measured by the buoy was 6.2 m/s.

When the minimum SGA is greater than 6° or 7°, the model slopes are not monotonic, and may produce ambiguous solutions. This is an inherent feature of the reflectance behavior, described by the Cox–Munk model: for a specified wind speed, the reflectance vs. view zenith angle curve may appear either high and narrow or short and broad, depending upon the minimum SGA. Fig. 7 shows normalized width slopes for the 16 modeled wind speeds, for the 3.6 m/s case illustrated in Fig. 4, plotted against their associated wind speeds and connected with a curved line. The 0 m/s model wind speed has an out-of-sequence, higher slope as a result of the transition with increasing minimum SGA discussed above. This transition is evident even at 9.49°, a comparatively low minimum SGA.

For ambiguous cases, if the retrieved wind speeds are within 1 or 2 m/s, we select the model closest to the observation. If the observed slope crosses the model curve at significantly different wind speeds, absolute reflectance is used to resolve the ambiguity. The minimum reflectances among the nine MISR views and among the nine model values are compared, for candidates on each branch. The wind speed associated with the closest match between model and observed minimum reflectance is selected. Physically, this procedure relies on the fact that the minimum reflectance generally increases with wind speed, since, as the surface roughens, the light is spread more uniformly with view angle. It is a qualitative indicator, but it is sufficient to identify a unique wind speed result correctly for 14 of the 17 ambiguous events in our validation data set. In general, simply selecting the solution based on comparing the observed and modeled minimum reflectance values was found to be more reliable than using cubic spline interpolated minimum reflectance values.

The MISR-observed slope can be smaller than all the modeled values, as illustrated in Fig. 8. There is no ambiguity in such cases, since the observed slope falls below 2 m/s, the smallest value produced by the simulation. This is a low-wind situation, for which the measured wind speed was 3.0 m/s; the gap between the simulated and observed slopes is a measure of the method's uncertainty.

3.4. Overall assessment of retrieval results

Our goal is to develop a method for determining the wind speed from MISR observations alone, since for most MISR observations over ocean, there is no buoy data providing coincident wind speeds. Using the entire data set studied here, we assess the overall accuracy of the MISR wind speed retrieval described in Section 3.3. The validation results will depend on the angular coverage of the satellite observations relative to the specular direction (measured by the magnitude of the minimum SGA), the wind speed itself, and the degree to which the buoy measurement represents the time-averaged wind speed that drives ocean surface roughness.

Wind speeds retrieved from MISR observations compare favorably with surface wind speed measurements from moored ocean buoys, up to a minimum SGA of about 15°. Figs. 9 and 10, and Table 2, summarize the results. In Fig. 9, cases having minimum SGA less than 15° are displayed as filled circles, and those with minimum SGA greater than 15° are shown as X's. In Fig. 10, cases having minimum SGA less than 15° are displayed as solid bars, and those with minimum SGA greater than 15° are shown as outlined bars. Table 2 is also organized by minimum SGA.

Of the 38 data sets collected, 20 meet the minimum SGA condition. Fourteen of these, well distributed between 3.0 and 10.3 m/s and having minimum SGA ranging from 6.5° to 14.1°, produced wind speeds within 1 m/s of the corresponding surface measurement; four events, between 2.1 and 8.7 m/s and having minimum SGA between 11.5° and 13.9°, produced wind speeds within 1.5 m/s. In one case, for which the buoy-measured wind speed was 6.6 m/s and the minimum SGA was 13.1°, the MISR-retrieved value differed from the buoy measurement by 2.4 m/s,

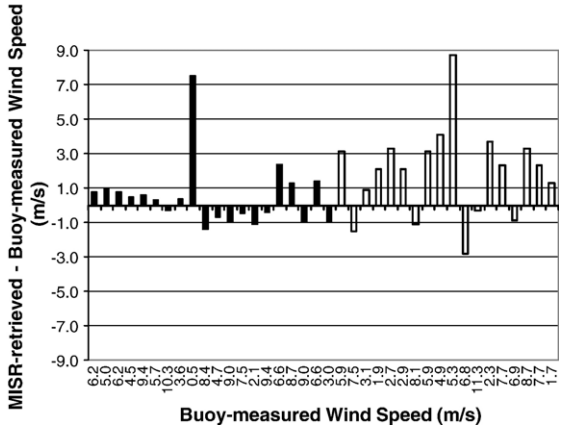

Fig. 10. Bar chart showing the differences between the MISR-retrieved and buoy-measured wind speeds for all 38 cases, ordered by minimum SGA. Cases having minimum SGA less than 15° are displayed as solid bars, and cases having minimum SGA greater than 15° are displayed as outlined bars.

Table 2
Wind speed retrieval performance for the 38 events in this studysuper †

Minimum SGA	MSIR orbit	NOAA buoy	NOAA buoy location		Height of wind speed measurement from buoy over ocean surace (m)	Buoy observed wind speed (m/s)	MISR retrieved wind speed (resolved if ambiguous) (m/s)	[MISR Retrieved − Buoy Observed] wind speed (m/s)	Ambiguous?
			Lat (°)	Long (°)					
6.4528	2410	51028	0	−153.88	5	6.2	7.0	0.8	No
7.8236	3779	51004	17.52	−152.48	5	5.0	6.0	1.0	No
8.3628	2177	51028	0	−153.88	5	6.2	7.0	0.8	No
8.367	3109.0	51028	0	−153.88	5	4.5	5.0	0.5	No
8.8379	3545	46042	36.75	−122.42	5	9.4	10.0	0.6	No
9.2631	1930	51001	23.43	−162.21	5	5.7	6.0	0.3	No
9.4638	14627	46062	35.10	−121.01	5	10.3	10.0	−0.3	No
9.4938	14525	46053	34.24	−119.85	5	3.6	4.0	0.4	0, 1, 4→4
11.073	2221	51002	17.15	−157.79	5	0.5	8.0	7.5	No
11.489	13580	51001	23.43	−162.21	5	8.4	7.0	−1.4	0, 1, 7→7
12.06	12648	51001	23.43	−162.21	5	4.7	4.0	−0.7	0, 1, 4→4
12.064	13813	51001	23.43	−162.21	5	9.0	8.0	−1.0	0, 1, 8→8
12.101	3561	51001	23.43	−162.21	5	7.5	7.0	−0.5	0, 1, 7→7
12.233	10216	51003	19.16	−160.74	5	2.1	1.0	−1.1	0, 1, 3→1
12.59	3153	51002	17.15	−157.79	5	9.4	9.0	−0.4	0, 1, 9→9
13.052	3545	46012	37.36	−122.88	5	6.6	9.0	2.4	0, 1, 9→9
13.476	3575	51028	0	−153.88	5	8.7	10.0	1.3	0, 1, 10→10
13.773	14046	51001	23.43	−162.21	5	9.0	8.0	−1.0	0, 1, 8→8
13.942	1216	51004	17.52	−152.48	5	6.6	8.0	1.4	0, 1, 8→8
14.116	14525	46054	34.27	−120.45	10	3.0	2.0	−1.0	No
16.302	1711	51028	0	−153.88	5	5.9	9.0	3.1	1, 2, 9→9
19.274	4740	51028	0	−153.88	5	7.5	6.0	−1.5	3, 4, 6→6
19.336	14525	46023	34.71	−120.97	10	3.1	4.0	0.9	No
19.514	14525	46011	34.88	−120.87	5	1.9	4.0	2.1	No
20.46	14860	46028	35.74	−121.89	5	2.7	6.0	3.3	No
21.265	14525	46062	35.10	−121.01	5	2.9	5.0	2.1	No
25.823	8599	51028	0	−153.88	5	8.1	7.0	−1.1	No
27.627	9296	51004	17.52	−152.48	5	5.9	9.0	3.1	7, 9→9
29.371	10201	51004	17.52	−152.48	5	4.9	9.0	4.1	No
29.627	14525	46028	35.74	−121.89	5	5.3	14.0	8.7	6, 14→14
29.722	4405	51028	0	−153.88	5	6.8	4.0	−2.8	No
30.675	1347	51004	17.52	−152.48	5	11.3	11.0	−0.3	8, 11→11
30.719	15342	51001	23.43	−162.21	5	2.3	6.0	3.7	6, 15→6
31.226	7216	51003	19.16	−160.74	5	7.7	10.0	2.3	No
32.621	4638	51028	0	−153.88	5	6.9	6.0	−0.9	No
34.05	1420	51002	17.15	−157.79	5	8.7	12.0	3.3	No
34.209	9779	51003	19.16	−160.74	5	7.7	10.0	2.3	No
35.855	12138	51002	17.15	−157.79	5	1.7	3.0	1.3	No
								RMS=2.60	

†"Ambiguous" refers to situations where the curve of model slopes as a function of wind speed crosses the observed slope at more than one point (e.g., Fig. 7). These cases are resolved using the minimum observed absolute reflectance value, as described in Section 3.3.

and in the final case, having 0.5 m/s wind speed and minimum SGA 11.1°, the results differed by 7.5 m/s. We could not identify a specific cause for this one significant anomaly among the retrievals; it is likely caused by small deformations of the nearly flat ocean surface.

For minimum SGA greater than 15° the retrieval is less reliable because the glint pattern is poorly sampled by the MISR observations. Frequent discrepancies of 3–4 m/s occur, and one error is as high as 8.7 m/s, although there are also several quite accurate retrievals.

Table 2 also summarizes the algorithm's ability to resolve ambiguous solutions. The final column lists the candidate wind speeds, and, following the arrow, reports the retrieved wind speed, obtained as described in the previous section. The method provides accurate resolutions for fourteen of seventeen cases, covering virtually the full range of minimum SGA. Only one failure occurs at a minimum SGA less than 15°, and that case produced an error of only 1.1 m/s, in the retrieved wind speed, well within the expected uncertainty of the retrieval. Fig. 10 displays all the MISR Retrieved − Buoy Observed wind speed differences.

The overall success of this approach at estimating wind speeds ranging from 2.1 m/s to 10.3 m/s, whenever MISR adequately samples the glint pattern (minimum SGA below 15°), also provides evidence of the Cox–Munk model's accuracy for natural ocean surface conditions.

4. Conclusions

In this paper, we explored the relationship between the MISR-observed width of the sun glint pattern over ocean and the near-surface wind speed. We used this relationship to develop an algorithm that can constrain the standard, wind-driven glint/white cap model defining the ocean–surface boundary condition in MISR aerosol retrievals. We adopted the Cox–Munk ocean surface model (Cox & Munk, 1954) to analyze glint pattern dependence on wind speed, first by simulating multi-angle reflectance curves for each MISR observation geometry, over a range of wind speeds, and then by calculating the slope of the glint peak's incrementally measured, normalized widths, as a function of wind speed. The retrieval amounted to identifying the model slope most closely matching that observed by MISR. Using coincident buoy data as ground truth, we demonstrated that the key geometric factor determining wind retrieval quality is the angular distance between the reflection vector and the closest MISR multi-angle observation — the minimum Sun Glint Angle (SGA).

MISR-retrieved winds are within 2.4 m/s of the buoy-measured values, and usually better than 1.1 m/s, for minimum SGA below about 15° among the cases studied, except one for which the wind speed was extremely low. For minimum SGA above about 15°, MISR angular sampling of the glint pattern reflectance is not adequate to perform meaningful wind retrievals.

For minimum SGA above 6° or 7°, one subtlety is that the glint-reflectance slope criterion used to identify solutions may not be unique. We resolve this ambiguity by taking account of the minimum observed absolute reflectance among the nine MISR view angles, a quantity that increases as higher wind speeds roughen the ocean surface, scattering light more broadly with view angle. This is a relatively crude wind speed result, but it meets our objective of providing an adaptive procedure for extracting, as best we can, some information about sea state from the MISR data itself, to constrain the white cap model. Our alternative is to continue using only the monthly, global $1° \times 1°$ wind speed climatology, which of course misses all severe events, inter-annual variability, etc. And there are no near-coincident satellite scatterometers that could provide more tightly constrained wind results. Other meteorological models would be expensive to implement, and would not necessarily provide better information for this particular application.

The validation process also demonstrated the high accuracy of the Cox–Munk ocean surface reflectance model. The wind-retrieval method derived here could be used in an operational multi-angle aerosol retrieval algorithm to dynamically constrain the ocean surface boundary condition when glint pattern angular sampling is adequate. An instrument having finer angular resolution could retrieve wind direction as well as wind speed (e.g., Breon & Henriot, 2006), and having broader angular coverage would increase the fraction of observations for which the 15° minimum SGA criterion is achieved.

Acknowledgements

We thank our colleagues on the Jet Propulsion Laboratory's MISR instrument team and at the NASA Langley Research Center's Atmospheric Sciences Data Center for their roles in producing the MISR data sets, and NOAA's National Data Buoy Center for providing the key validation data used in this study. We also thank Dave Diner for suggesting that we look at the slopes of the widths/peak height ratios for the modeled and MISR curves, Barbara Gaitley for producing the MISR base maps used in Fig. 1a and b, the Student Independent Research Internship (SIRI) and Research Apprenticeship (RA) Programs at JPL for providing D.F. and E.G. an opportunity to work with JPL scientists, and Professor Rick Guglielmino of Glendale College for his academic support during the project. This research is supported in part by NASA's Climate and Radiation Research and Analysis Program, under H. Maring, NASA's Atmospheric Composition Program under P. DeCola, and the EOS–MISR instrument project. It is performed at the Jet Propulsion Laboratory, California Institute of Technology, under contract with NASA.

References

Breon, F. M., & Henriot, N. (2006). Spaceborne observations of ocean glint reflectance and modeling of wave slope distributions. *Journal of Geophysical Research*, *111*, C06005, doi:10.1029/2005JC003343.

Cox, C., & Munk, W. (1954). Statistics of the sea surface derived from Sun glitter. *Journal of Marine Research*, *13*, 198−227.

Diner, D. J., Beckert, J. C., Reilly, T. H., Bruegge, C. J., Conel, J. E., Kahn, R., et al. (1998). Multiangle Imaging SpectroRadiometer (MISR) description and experiment overview. *IEEE Transactions on Geoscience and Remote Sensing*, *36*, 1072−1087.

Frouin, R., Schwindling, M., & Deschamps, P. -Y. (1996). Spectral reflectance of sea foam in the visible and near-infrared: In situ measurements and remote sensing implications. *Journal of Geophysical Research*, *101*, 14,361−14,371.

Kahn, R., Banerjee, P., McDonald, D., & Martonchik, J. (2001). Aerosol properties derived from aircraft multi-angle imaging over Monterey Bay. *Journal of Geophysical Research*, *106*, 11977−11995.

Koepke, P. (1984). Effective reflectance of oceanic whitecaps. *Applied Optics*, *23*, 1816−1824.

Martonchik, J. V., Diner, D. J., Kahn, R., Verstraete, M. M., Pinty, B., Gordon, H. R., et al. (1998). Techniques for the Retrieval of aerosol properties over land and ocean using multiangle imaging. *IEEE Transactions on Geoscience and Remote Sensing*, *36*, 1212−1227.

Moore, K. D., Voss, K. J., & Gordon, H. R. (2000). Spectral reflectance of whitecaps: Their contribution to water-leaving radiance. *Journal of Geophysical Research*, *105*, 6493−6499.